HiSST: 3rd International Conference on
High-Speed Vehicle Science Technology
14 -19 April 2024, Busan, Korea

# Effectiveness-NTU Model for PCM-Compact Heat Exchanger Performance Prediction

*J. Y. Frank [1], D. J. Borman [2], A. Khan [2], E. Greiciunas [3], J. Summers [4,5]*

## Abstract

One of the limiting factors for the development of future aircraft is the size of thermal management systems. The addition of Phase Change Materials (PCM) heat exchangers has been identified as a potential improvement to the system, where the PCM heat exchanger would help in reducing peaks in the heat load, extending the lifetime of current technologies. There is a current lack of low computational cost models suited for the initial sizing phase of PCM-Compact heat exchangers. An effectiveness-NTU model has been developed that tracks the melting/solidification front of the PCM by using a linear approximation of the Stefan Condition. Based on an initial loading profile characteristic of aerospace applications, the model is applied to a PCM-Compact heat exchanger. The model results are in good agreement with three-dimensional CFD results that are used for comparison and achieve a clear reduction in the simulation time from multiple hours to seconds per loading case when comparing the model to CFD simulations.

**Keywords: Thermal Storage, Phase Change Materials, Compact Heat Exchanger, Effectiveness-NTU model.**

## Nomenclature

Latin
$A$ – Heat transfer surface area [m$^2$]
$A_{fin}/A_T$ – Fin area over total area
$a$ – Melting thickness of PCM [m]
$b$ – Plate Spacing [mm]
CFD – Computational Fluid Dynamics
$c_p$ – Specific heat capacity [J/kgK]
$D_h$ – Hydraulic diameter [m]
$h$ – Sensible enthalpy [J/kg]
$h_f$ – Fluid heat transfer coefficient [W/m$^{-2}$K]
$j$ – Colburn factor
$k$ – Thermal conductivity [W/mK]
$L$ – Latent heat of fusion [kJ/kg]
$\dot{m}$ – Mass flow rate [kg/s]
Nu – Nusselt number, $Nu = hL/k$
$NTU$ – Number of Transfer Units
$p$ – Pressure
PCM – Phase Change Material
Pr – Prandtl number, $\mathrm{Pr} = \nu/\alpha$
Re – Reynolds number, $\mathrm{Re} = (D_h \dot{m})/(A_c\, \mu_f)$
$S_h$ – Latent Heat Source Term
$T$ – Temperature [K]
TMS – Thermal Management System
$t_w$ – Wall thickness [m]
$u$ – Velocity [m/s]
$U$ – Overall heat transfer coefficient [W/m$^{-2}$K]

Greek
$\beta$ – Heat transfer area/ volume between plates [m$^3$/m$^2$]
$\delta$ – Fin Thickness [m]
$\Delta H$ – Latent heat enthalpy [J/kg]
$\epsilon$ – Effectiveness
$\phi$ – Liquid Fraction
$\eta_0$ – Surface effectiveness
$\mu$ – Kinematic viscosity [mPa.s]
$\rho$ – Density [kg/m$^3$]

[1] *Centre for Doctoral Training in Fluids Dynamics, University of Leeds, Woodhouse, Leeds, LS2 9JT, United Kingdom, mn17jyf@leeds.ac.uk.*
[2] *School of Civil Engineering, University of Leeds, Woodhouse, Leeds, LS2 9JT, United Kingdom.*
[3] *Ignitis, Laisvės pr. 10, LT-04215 Vilnius, Lithuania*
[4] *School of Mechanical Engineering, University of Leeds, Woodhouse, Leeds, LS2 9JT, United Kingdom.*
[5] *Research Institutes of Sweden (RISE), Traktorvägen 1, 973 47 Luleå, Sweden.*

Subscripts
in – Inlet
out – Outlet
f – Fluid
l – Liquidus
s – Solidus
w - Wall
PC – Phase Change

## 1. Introduction

The growing thermal load in aircraft design poses challenges to the development of compact thermal management systems (TMS) for future-generation aircraft. This in part can be attributed to the increase in onboard avionics systems, leading to more low-quality heat being produced inside the aircraft, as well as the growing use of composite materials, which can reduce heat losses to the atmosphere via the airframe structure [1]. To manage this increase in heat load of future aircraft, the TMS will have to be improved or adjustments will have to be made to the heat exchanger designs.

The use of Phase Change Materials (PCM) as part of the TMS has been identified as a viable solution to this problem [1]. PCMs absorb and release heat at almost constant temperature and could be used to absorb the energy at key stages of the flight, when the load on the TMS is more pronounced, such as take-off, maneuvers, and landing. The remaining components of the TMS could then be designed around a lower averaged head load so that a reduction in the size of the main heat exchanger might be achieved.

PCMs have been successfully applied for numerous cooling applications in civil engineering projects [2, 3]. This trend is primarily influenced by the low thermal conductivity of most PCMs, resulting in gradual heat absorption and release rates that align well with the daily thermal fluctuations these units are designed to manage. To limit operating costs due to pumping power, simple designs are selected, such as shell and tube configurations, where the PCM is stored in the shell, with a heat transfer fluid (HTF) circulating inside the tubes [4, 5]. Another popular configuration is plate heat exchangers, where the PCM is stored in slabs [6]. Various heat exchanger performance enhancement techniques have been investigated, where the low thermal conductivity of the PCM can be balanced by introducing metal fins, screens and spheres into the PCM [7–9], or by creating a PCM-porous foam material [10, 11].

Computational Fluid Dynamics (CFD) emerges as a powerful tool for modelling the melting inside of PCM heat exchangers [12]. In shell and tube heat exchangers, the underlying physics of melting and solidification of PCM are complex, leading to modelling challenges. The large diameter of the shell and tube units leads to convection in the pool of liquid PCM, which increases the melting rate of the PCM. On top of this, the phase change occurs over a small range of temperatures, forming a mushy zone in which one part of the PCM is solid and the other is liquid. This influences the velocity within that area so that the average velocity decreases as the PCM solidifies. This needs to be properly accounted for when modelling the phase change process to accurately predict the performance of the heat exchanger. Multiple models have been proposed and validated against experimental results, such as the enthalpy-porosity approach [13] or the effective heat capacity method [14]. In these models, the solid and liquid phases are modelled as one computational domain, allowing for a fixed grid to be used. The models are widely available in both commercial and open-source software, enabling the investigation of various operating conditions and geometries on the heat transfer performance to be reviewed in [4].

However, CFD is computationally expensive, as a fine mesh is needed to resolve complex geometries and small timesteps are required to fully capture the complex physics of the problem. Simulations of shell and tube heat exchangers in the literature are often limited to 2D, where only the melting or solidification of the PCM is modelled by imposing a heat flux or constant temperature boundary condition at the walls. As a result, the effect of the temperature drop of the HTF over the length of the heat exchanger on the heat absorption rate of the PCM is rarely considered in the literature. Nonetheless, studies acknowledging this factor have shown a considerable impact on the melting rate [14,15]. This can make CFD unsuitable for the initial sizing process of a heat exchanger, where it is important to assess a wide range of geometries or operating conditions on the effectiveness of the heat exchanger.

To overcome this issue, several analytical models based on the effectiveness-NTU ($\epsilon - NTU$) model have been proposed for PCM shell and tube [15–18] and plate heat exchangers [19]. The models have shown good agreement with experimental and numerical results, while significantly reducing the computational cost so that they can be applied to parametric studies and design optimization.

In the case of a heat exchanger with PCM, it is challenging to find an analytical solution to this problem due to the solid/liquid interface moving over time as the PCM melts or solidifies. The simplest way of tackling this issue is by introducing a time-independent phase change fraction parameter, which can be used to calculate an average effectiveness value [15, 16, 19]. In this way, the exact position of the solid/liquid interface over time is not required to determine the performance of the heat exchanger from the temperature drop of the HTF. This method was extended by Tay et al. [20] to incorporate radial fins in the model. However, the method is not fully suitable for the initial sizing process as it is not possible to determine whether the PCM will be fully melted or solidified in the available period from the model. Therefore, additional experimental or numerical studies would need to be completed to determine the melting rate of the PCM. This problem is addressed in Tian et al. [18], where the position of the PCM front is determined by using the Stefan condition, where additional thermal energy at the melt interface is balanced by the heat absorbed by the melting front. The resulting model is built upon energy conservation where the $\epsilon - NTU$ model is coupled to the 1D Stefan Condition by assuming that all the heat released by the HTF is absorbed by the PCM in the form of latent heat. This leads to an ODE that must be solved numerically, leading to an increase in computational cost when compared to the simpler phase change fraction approach, but this now allows for the use of more complex transient operating conditions.

The loading profile for aerospace favours a reduction of the melting time and the mass of the system to limit the operating costs of the aircraft, which cannot be achieved efficiently with the simple geometries previously considered in most of the literature. For conventional heat exchangers, this is achieved by using more compact geometries, where the heat transfer surface area of the heat exchanger is increased. Geometries such as plate-fin and tube-fin heat exchangers are commonly applied in this case. The literature on PCM-Compact heat exchanger (PCM-CHX), where fins are added on the HTF side is limited. The work of Stathopoulos et al. [21, 22] and Barz and Emhofers [23] covers Air-PCM fin-plate heat exchanger geometries. Shon et al. [24] and Promoppatum et al. [25] focus on fin-tube heat exchangers.

This paper builds upon an $\epsilon - NTU$ model for PCM-CHX previously proposed by the current authors in [26], where the $\epsilon - NTU$ model shares similarities with the model proposed by Tian et al. [18]. However, instead of solving an ODE, the Stefan condition is linearized in the current model. In this paper, the model is validated by comparing the output with CFD simulations for a plate-fin compact heat exchanger geometry.

## 2. Materials and Methods

### 2.1. Heat exchanger geometry

The PCM heat exchanger considered in this work consists of layers of offset stripped fins (1/8-13.95 [27], see Table 1 for fin properties) through which the fluid will flow and layers of PCM separated from the fluid layer by plates (see Fig. 1). The length of the heat exchanger is chosen based on 10 periodic lengths of stripped fins, leading to a length of 63.5 mm.

**Table 1.** Properties of offset stripped fins (1/8-13.95) [27]

| Fin Property | |
|---|---|
| Fluid plate spacing ($b_f$) (mm) | 9.525 |
| Hydraulic Diameter ($D_h$) (mm) | 2.68 |
| Fin pitch (/m) | 549 |
| Fin Thickness ($\delta$) (mm) | 0.254 |
| Fin Length (mm) | 3.175 |
| Heat transfer area/ volume between plates ($\beta$) ($m^2/m^3$) | 1250 |
| Fin area/Total area ($A_{fin}/A_T$) | 0.840 |

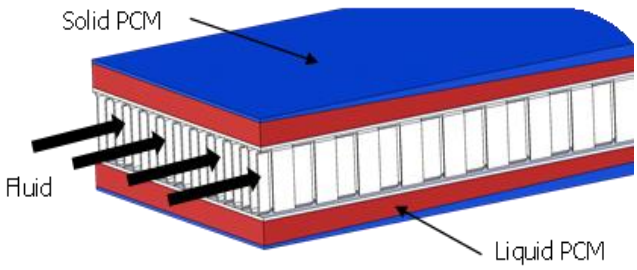


**Fig. 1.** Geometry of heat exchanger with 1/8-13.95 fins

### 2.2. Material Properties and Operating Conditions

Water is used as the heat transfer fluid, the PCM is taken to be RT18 HC, and the fins and separating plate are made of aluminium. The material properties for these are described in Table 2. For the melting cycle, the fluid enters the heat exchanger with a temperature of 301.15 K for a total period $t_{end}$ of 100 s, such that there is a 10 K difference between the inlet temperature and the phase change temperature of the PCM. Due to these operating conditions, the thickness of PCM will be relatively small, so that the Rayleigh number in the PCM layer will remain below the critical value, which has been identified to be between 1296 and 1708 [28, 29]. As a result, buoyancy in the liquid PCM is neglected in the model and the melting and solidification cycle will behave similarly if the temperature difference between the inlet and the phase change temperature is equivalent. Only the melting cycle will be considered here. The heat exchanger operates at a Reynolds number $\mathrm{Re} = 200$, where the Reynolds number was chosen based on the hydraulic diameter $D_h$ and free flow area $A_c$ of the finned surface, the mass flow rate $\dot{m}$ and viscosity $\mu$ of the fluid:

$$\mathrm{Re} = \frac{D_h \dot{m}}{A_c \, \mu_f} \tag{1}$$

**Table 2.** Material properties (RT18 HC material properties provided by the manufacturer)

| Material Property | Water | RT18 HC | Aluminium |
|---|---|---|---|
| Density $\rho$ (kg/m3) | 998.2 | 770 | 2719 |
| Dynamic Viscosity $\mu$ (mPa.s) | 1.0016 | - | - |
| Specific heat capacity $c_p$ (J/(K kg) | 4184 | 2000 | 871 |
| Thermal conductivity (W/(m K)) | 0.6065 | 0.2 | 202.4 |
| Latent Heat of Fusion $L_{PCM}$ (kJ/kg) | - | 260 | - |
| Phase Change Temperature $T_{PC}$ (K) | - | 290.15-292.15 | - |

### 2.3. Effectiveness-NTU model

Fig. 2 shows the heat transfer problem for a PCM-CHX. The hot fluid flowing in the adjoining channel to the PCM will start the melting process, so that the thickness of melted PCM ($a$) increases over time. During the phase change, the PCM absorbs the heat from the fluid in the form of latent heat, leading to a decrease of the fluid temperature over the length of the heat exchanger. This leads to a decrease in the melting rate further along the length of the heat exchanger, such that $a$ is smaller at the outlet when compared to the inlet. This problem can be represented by an effectiveness-NTU model, where the effectiveness ($\epsilon$) is the ratio between the actual heat flux over the maximum possible heat flux. For a PCM heat exchanger, it is assumed that the PCM acts as a perfect heat sink and that all the heat stored in the PCM is stored as latent heat. Making this assumption results in a perfect heat sink problem, where the solid/liquid interface is kept at a constant temperature $T_{PC}$ and moves over time. As such, the effectiveness can be expressed as:

$$\epsilon = \frac{T_{in} - T_{out}}{T_{in} - T_{PC}}. \tag{2}$$

where, $T_{in}$ and $T_{out}$ are the fluid inlet and outlet temperatures respectively. The effectiveness is related to the Number of Transfer Units (NTU) and can be expressed in this case as:

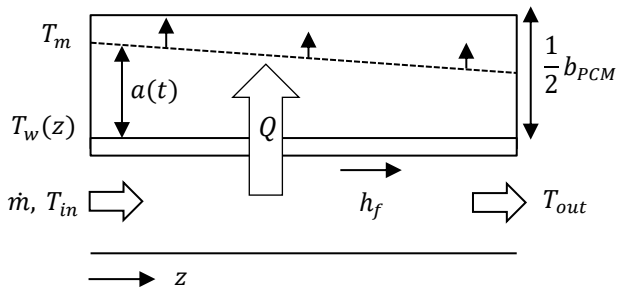


**Fig. 2.** Geometry of Heat Exchanger with 1/8-13.95 fins

$$\epsilon = 1 - \exp(-\mathrm{NTU}), \tag{3}$$

where the NTU can be determined from the overall heat transfer coefficient ($U$):

$$NTU = \frac{UA_f}{\dot{m}c_p}, \tag{4}$$

where, $A_f$ is the heat transfer surface area on the fluid side and $c_p$ is the specific heat capacity of the fluid.

The overall heat transfer coefficient ($U$) can then be calculated from a simple thermal circuit representing the finned surface on the fluid side, the wall and the PCM side. The heat transfer on the PCM side is dominated by conduction, so that all effects of buoyancy within the melted pool are neglected. As such, $U$ is defined as:

$$U = \left[\frac{1}{\eta_{0,f} h_f} + \frac{t_w}{\frac{A_w}{A_f} k_w} + \frac{a(t)}{\frac{A_{PCM}}{A_f} k_{PCM}}\right]^{-1}, \tag{5}$$

where $\eta_{0,f}$ is the surface effectiveness of the fin, due to the drop in temperature along the height of the fin (see Kays and London [27] for a full explanation on how to calculate the surface effectiveness for compact heat exchangers), $h_f$ is the heat transfer coefficient of the fluid, which can be determined from experimental or numerical data as shown in Figure 7. $t_w$ and $a$ are the thickness of the wall and the melted PCM respectively, $A_w$, $A_f$ and $A_{PCM}$ are the surface areas of the wall the fluid and the PCM respectively and $k_w$, $k_{PCM}$ are the thermal conductivities of the wall and PCM respectively. Note that the overall heat transfer coefficient is dependent on the melting thickness that will increase in time, increasing the complexity of the model.

### 2.4. The Stefan Condition

The Stefan Condition for a one dimensional problem can be used to accurately predict the position of the melting front in the $\epsilon - NTU$ model:

$$\rho_{PCM} L_{PCM} \frac{da}{dt} = k_{PCM} \left.\frac{\partial T}{\partial y}\right|_{y=a^-}, \tag{6}$$

where $\rho_{PCM}$ is the density of the PCM and $L_{PCM}$ is the latent heat of fusion of the PCM. For large Stefan number, the velocity of the solid/liquid interface $\frac{da}{dt}$ is low, so that the heat transfer in the PCM is quasi-steady. In this case, equation (6) can be simplified to:

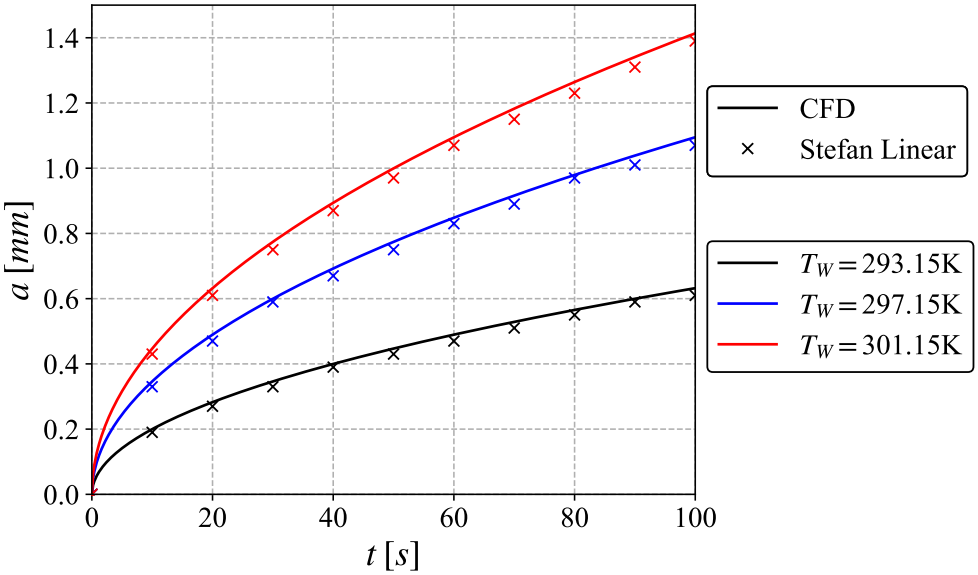


**Fig. 3.** Comparison of the melting thickness ($a$) over time for the linearized Stefan condition against a 1D CFD model for different wall temperature input ($T_w$) for RT18 HC.

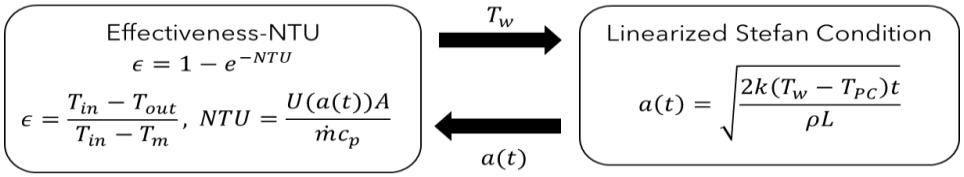


**Fig. 4.** Summary of PCM-Effectiveness-NTU model

$$a(t) = \sqrt{\frac{2k_{PCM}(T_w - T_{PC})t}{\rho_{PCM} L_{PCM}}}, \tag{7}$$

where $T_w$, is the wall temperature and $T_{PC}$ is the phase change temperature, which will be taken as half the melting range ($T_{PC} = 291.15\,K$ for RT18 HC) [26]. Fig. 3 shows the melting thickness prediction from the linearized Stefan condition against 1D CFD results over time, where the CFD results are obtained from the enthalpy model described in Section 2.5. Good agreement is observed between the CFD and the linearized Stefan Condition, where the melting thickness is a bit higher for the CFD.
Note that the melting thickness requires the knowledge of the wall temperature, which needs to be deduced from the temperature drop. Assuming that the system behaves as a steady state system, this can be obtained from the bulk temperature and the overall heat transfer coefficient contribution of the fluid and wall:

$$T_w = T_B - q\left(\frac{1}{\eta_{0,f} h_f A_f} + \frac{t_w}{k_w A_w}\right) \tag{8}$$

A summary of the PCM $\epsilon - NTU$ model is provided in Fig. 4. As the fluid temperature drops over the length of the heat exchanger, this will lead to a decrease of the PCM thickness over the length of the heat exchanger. This can be taken into account by the $\epsilon - NTU$ model by splitting the length of the heat exchanger into elements and by predicting a local temperature drop and corresponding melting thickness at that point [26]. A visual summary is shown in Fig. 5.

### 2.5. CFD model

A 3D CFD model of the PCM-Compact heat exchanger was created in Ansys FLUENT to validate the $\epsilon - NTU$ model. The phase change in the PCM is modelled by using an enthalpy model assuming laminar, transient, and fully conductive heat flux, such that there is no convection within the liquid pool of PCM:

$$\frac{\partial \rho h}{\partial t} = \boldsymbol{\nabla} \cdot (\mathrm{k}\,\boldsymbol{\nabla}\mathrm{T}) + S_h, \tag{9}$$

where $h$ is the sensible enthalpy ($h = h_{ref} + \int_{T_{ref}}^{T} c_p dT$) and $S_h$ is a source term collecting the latent heat enthalpy ($\Delta H$) contribution:

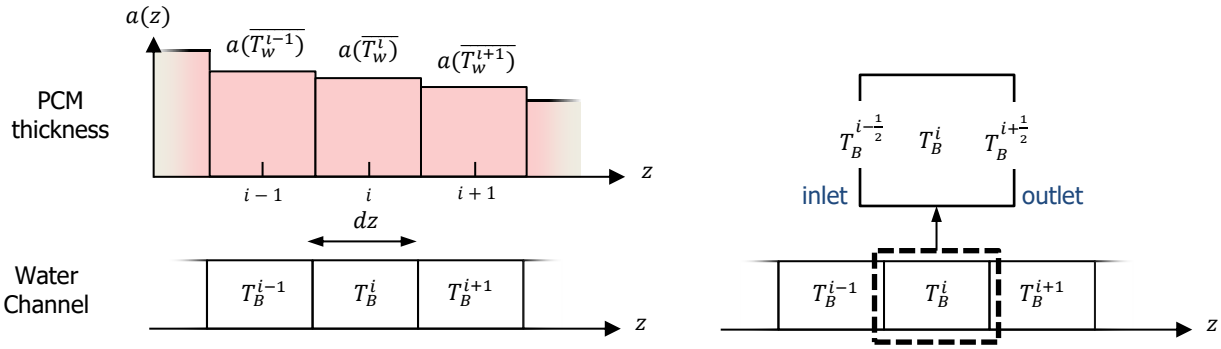


(a) Discretization of heat exchanger (b) Zoom on single element in fluid channel

**Fig. 5.** Discretization of the length of the heat exchanger into elements

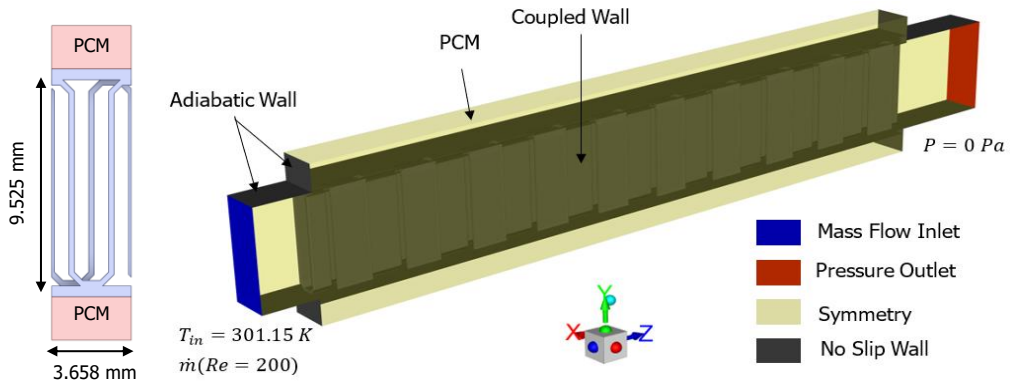


**Fig. 6.** Geometry and Boundary Conditions used for the CFD model.

$$S_h = -\frac{\partial \rho \Delta H}{\partial t}. \tag{10}$$

$\Delta H$ is defined in terms of the liquid fraction $\phi$ and the latent heat storage capacity $L$:

$$\Delta H = \phi L, \tag{11}$$

where:

$$\phi = \begin{cases} 0 & T < T_s, \\ \dfrac{T - T_s}{T_l - T_s} & T_s \leq T < T_l, \\ 1 & T \geq T_l. \end{cases} \tag{12}$$

To be able to account for the drop in the melting thickness due to the fluid temperature drop over the length of the heat exchanger, a conjugate heat transfer (CHT) approach was chosen. For this, only the conservation of energy equation is solved for the PCM (Eq. 9) in conjunction with the fluid (Eq. 13.a) and solid domain (Eq. 13.b) as:

$$\frac{\partial h}{\partial t} + \boldsymbol{\nabla} \cdot (\boldsymbol{u} h) = \boldsymbol{\nabla} \cdot (\alpha_{eff}\, \boldsymbol{\nabla} T). \tag{13.a}$$

$$\frac{\partial h}{\partial t} = \alpha_s\, \boldsymbol{\nabla}^2 T. \tag{13.b}$$

$\alpha$ is the thermal diffusivity, where $\alpha_{eff} = \alpha_f + \mu_t/(\rho \mathrm{Pr}_t)$ and $\mathrm{Pr}_t\mathrm{r}$ is the turbulent Prandtl number. Note that the convective heat transfer is considered in the fluid energy equation (13.a). To obtain the velocity vector field, a background fluid flow is separately obtained during an initial stage by solving for a steady-state, incompressible and laminar equation for continuity of mass (Eq. 14.a), momentum (Eq. 14.b).

$$\nabla \cdot \boldsymbol{u} = 0, \tag{14.a}$$

$$\rho_f (\boldsymbol{u} \cdot \nabla)\boldsymbol{u} = -\nabla \mathrm{p} + \mu_{eff}(\boldsymbol{\nabla u} + \boldsymbol{\nabla}^T \boldsymbol{u}), \tag{14.b}$$

with $\mu_{eff} = \mu_f + \mu_t$, where $\mu_t$ is the dynamic turbulent viscosity. Laminar flow was found to be sufficient for the low Reynolds number ($\mathrm{Re} = 200$) that was used as part of the validation process, such that $\mu_{eff} = \mu_f$ and $\alpha_{eff} = \alpha_f$ (see Fig. 7 for comparison of laminar and turbulent results). As part of the initialization stage, an initial temperature field is also obtained from a steady state solution for which the PCM temperature is set to a temperature below the solidus temperature. Here the initial PCM temperature was set to 290.14 K.

The geometry, operating conditions and material properties follow the methodology section in Section 2.1 and 2.2., with the final geometry and boundary conditions are summarized in Fig. 6.

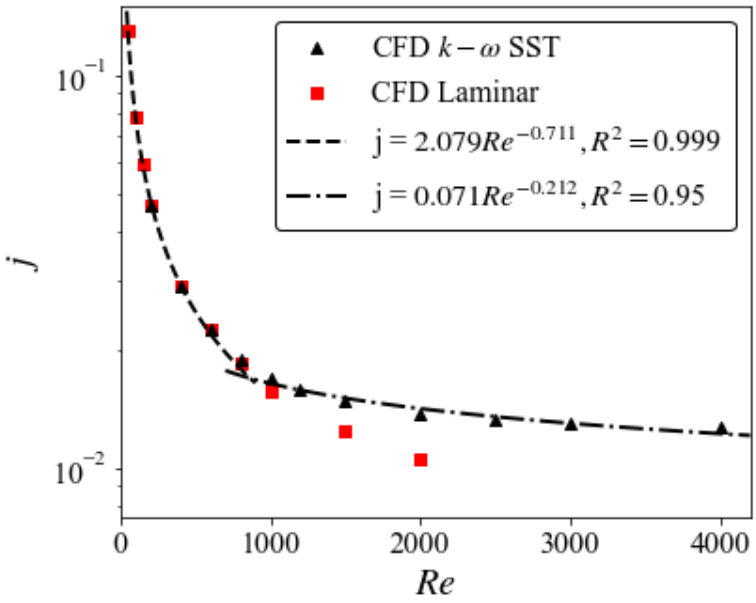


**Fig. 7.** J factor prediction from CFD model for laminar (■) and turbulent using $k-\omega\ SST$ model (▲).

### 2.6. Heat transfer coefficient prediction

The $\epsilon - NTU$ model requires a prediction of the heat transfer coefficient for the fluid domain. By using a single domain CFD model of the fluid channel, the Colburn (j) factor was calculated for the 1/8-13.95 strip fin geometry over a range of Reynolds number, $\mathrm{Re} \in [50; 4000]$.

Fig. 7 shows the predicted j factor obtained from the CFD for laminar and turbulent simulations, for which the $k-\omega\ SST$ model was used. This shows that the laminar assumption is valid up to $\mathrm{Re} < 850$, after which point the flow in the heat exchanger becomes turbulent. From the individual laminar data points, two power fit curves were created that can be used in the $\epsilon - NTU$ model:

$$\mathrm{j} = 2.079\ \mathrm{Re}^{-0.711} \qquad \text{for } \mathrm{Re} < 850, \tag{15.a}$$

$$\mathrm{j} = 0.071\ \mathrm{Re}^{-0.212} \qquad \text{for } \mathrm{Re} \geq 850. \tag{15.b}$$

The j factor is linked to the Nusselt number $\mathrm{Nu}$, Reynolds number $\mathrm{Re}$ and Prandtl number $\mathrm{Pr}$ by:

$$j = \frac{\mathrm{Nu}}{\mathrm{RePr}^{1/3}}, \tag{16}$$

which is linked to the heat transfer coefficient by:

$$h_f = \frac{k\mathrm{Nu}}{D_h} \tag{17}$$

## 3. Results and Discussion

### 3.1. Initial Condition used for CFD simulation.

A snapshot of the initial flow and temperature field in the fluid channel is shown in Fig. 8. The use of offset strip fins leads to a symmetric flow and temperature field with repeating flow features at every periodic length. This is attributed to the rapid mixing that occurs due to the periodic interruptions of the fins, such that the flow separates into two jets at the tip of the first fin, before rejoining in the wake of the fin. This leads to a considerable enhancement of the heat transfer, characteristic of the fin geometry, as the thermal boundary layer is consistently interrupted over the length of the heat exchanger. At $t = 0\ s$, the temperature drop is measured as $\Delta T = -3.8\ K$.

### 3.2. Comparison with $\epsilon - NTU$ model

The temperature drop in the fluid channel and the average liquid fraction are compared in Fig. 9 for the CFD and $\epsilon - NTU$ model results. Fig. 9.a. shows that the $\epsilon - NTU$ model is capable of accurately

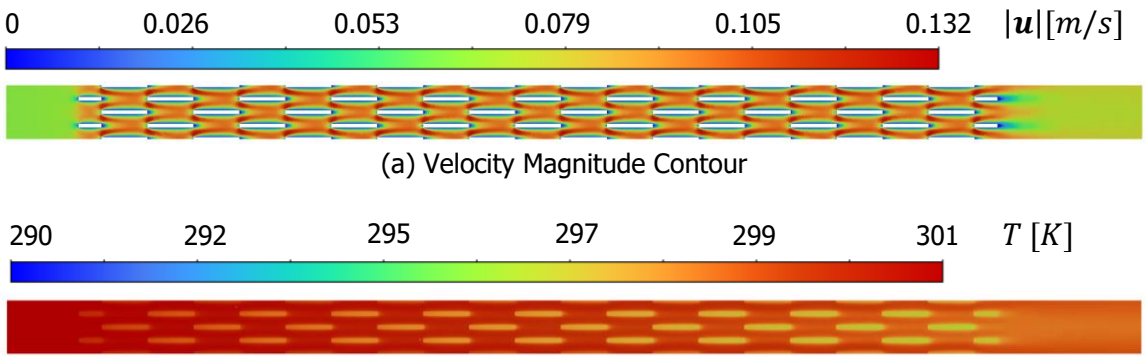


(a) Velocity Magnitude Contour

(b) Temperature Contour

**Fig. 8.** Contours of velocity magnitude (a) and temperature (b) at $\mathrm{Re} = 200$ showing the initial flow and temperature field in the fluid channel at the XZ plane for $y = 4.7625\ mm$ (halfway through the fluid domain).

predicting the temperature drop over time, and Fig. 9.b indicates that the model accurately captures the amount of latent heat that is stored within the PCM heat exchanger over time. A small difference in the temperature drop is observed in the first 10 s, where the temperature drop is seen to decrease more significantly for the $\epsilon - NTU$ model than for the CFD.

Fig. 10 shows the melting thickness over the length of the heat exchanger extracted from the CFD and $\epsilon - NTU$ model results over time. Good overall agreement is observed, with a maximum percentage difference of 4% between the two models. The $\epsilon - NTU$ model predicts a slightly higher melting thickness than the CFD, where the difference between the models increases with time.

The difference in results for the temperature drop and the melting thickness could be linked to the steady state nature of the $\epsilon - NTU$ model, such that the residence time of the fluid is not considered when predicting the temperature drop and the transient response of the heat exchanger is neglected. On top of this, the linearized Stefan condition was seen to predict a slightly higher melting thickness than the CFD in Fig. 3., which could have led to an increase in the difference when calculating the heat flux and wall temperature.

The temperature drop shown in Fig. 9.a shows that there is a significant decrease in the temperature drop in the first 10 s. Eq. 5 indicates that this is linked to the thermal resistance of the PCM dominating over the fluid and wall resistance. By introducing fins into the PCM, this would lead to a higher overall

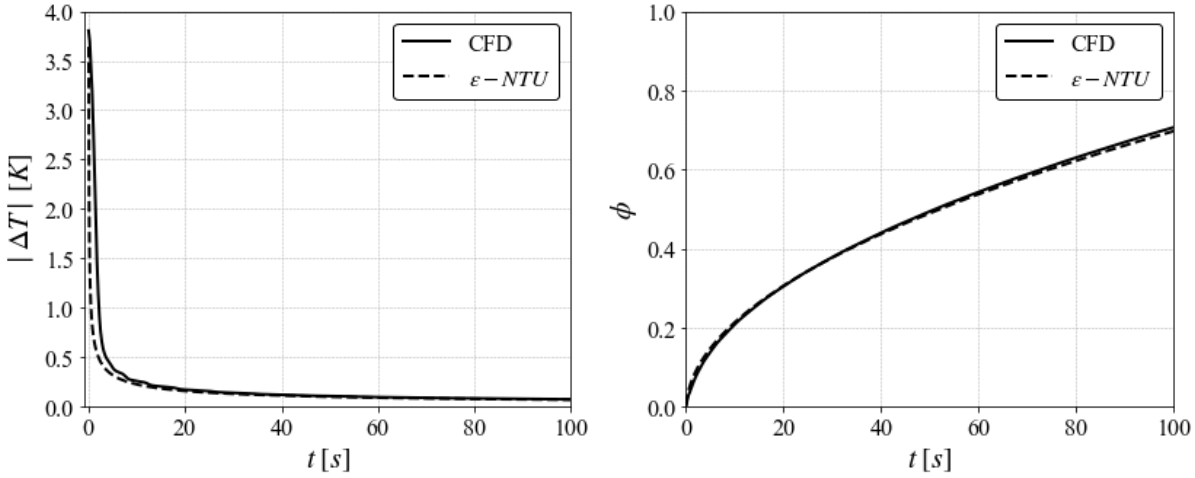


(a) Temperature Drop

(b) Liquid Fraction

**Fig. 9 :** Comparison of temperature drop ($|\Delta T|$) and average liquid fraction ($\phi$) over time for the CFD and $\epsilon - NTU$ model results.

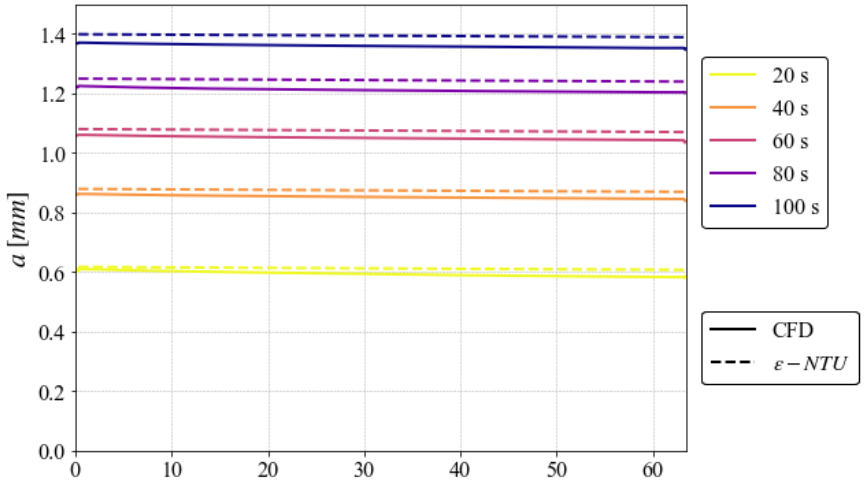


**Fig. 10:** Comparison of the prediction of the melting thickness ($\boldsymbol{a}$) over the length of the heat exchanger ($\boldsymbol{z}$) over time for the CFD and $\boldsymbol{\epsilon - NTU}$ model results. For CFD results, this is taken on the ZY plane at $\boldsymbol{x = 1.829\ mm}$ (halfway through the fluid domain).

thermal conductivity of the PCM such that more heat could be stored by the heat exchanger. When looking at the melting thickness plot in Fig. 10, it is possible to see that the drop in the melting thickness over the length is small. This is linked to the small temperature drop that is observed for most of the simulation time. Based on previous observations, this would suggest that adding fins to the PCM would lead to a less uniform distribution of the melting front.

## 4. Conclusion & Future work

A promising new semi-analytical model for the initial sizing of a PCM compact heat exchanger was presented in this paper. The model combines the $\epsilon - NTU$ method with a linear approximation of the Stefan Condition, leading to a significant reduction in computational cost when compared to CFD simulations. The model was compared against three-dimensional CFD simulation results for the melting of RT18 HC in an offset strip-fin geometry, where it was shown that the $\epsilon - NTU$ model was able to accurately predict the temperature drop of the fluid, the average liquid fraction, and the location of the solid/liquid interface over the length of the heat exchanger over time, appropriately predicting the amount of heat stored by the heat exchanger.

Currently, the model only incorporates fins in the fluid layer. Future work will involve the addition of fins in the PCM in the $\epsilon - NTU$ model, so that more effective designs can be evaluated by the model. The model could then be used to evaluate a large range of heat exchanger designs to identify an optimum geometry.

## Acknowledgements

This work was supported by the Engineering and Physical Sciences Research Council (EPSRC) Centre for Doctoral Training in Fluid Dynamics for the University of Leeds (Grant number EP/S022732/1). The CFD simulations were undertaken on ARC3, part of the High-Performance Computing facilities at the University of Leeds, UK. The project was conducted in partnership with BAE Systems and the authors would like to thank them for their support. For the purpose of open access, the author has applied a Creative Commons Attribution (CC BY) license to any Author Accepted Manuscript version arising from this submission. Data associated with this article is available upon request.

## References

1. van Heerden, A.S.J., Judt, D.M., Jafari, S., Lawson, C.P., Nikolaidis, T., Bosak, D.: Aircraft thermal management: Practices, technology, system architectures, future challenges, and opportunities. Progress in Aerospace Sciences. 128, 100767 (2022). https://doi.org/10.1016/j.paerosci.2021.100767

2. Akeiber, H., Nejat, P., Majid, M.Z.Abd., Wahid, M.A., Jomehzadeh, F., Zeynali Famileh, I., Calautit, J.K., Hughes, B.R., Zaki, S.A.: A review on phase change material (PCM) for sustainable passive cooling in building envelopes. Renewable and Sustainable Energy Reviews. 60, 1470–1497 (2016). https://doi.org/10.1016/j.rser.2016.03.036
3. Cabeza, L.F., Castell, A., Barreneche, C., de Gracia, A., Fernández, A.I.: Materials used as PCM in thermal energy storage in buildings: A review. Renewable and Sustainable Energy Reviews. 15, 1675–1695 (2011). https://doi.org/10.1016/j.rser.2010.11.018
4. Kalapala, L., Devanuri, J.K.: Influence of operational and design parameters on the performance of a PCM based heat exchanger for thermal energy storage – A review. Journal of Energy Storage. 20, 497–519 (2018). https://doi.org/10.1016/j.est.2018.10.024
5. Abdulateef, A.M., Mat, S., Abdulateef, J., Sopian, K., Al-Abidi, A.A.: Geometric and design parameters of fins employed for enhancing thermal energy storage systems: a review. Renewable and Sustainable Energy Reviews. 82, 1620–1635 (2018). https://doi.org/10.1016/j.rser.2017.07.009
6. Pereira da Cunha, J., Eames, P.: Thermal energy storage for low and medium temperature applications using phase change materials – A review. Applied Energy. 177, 227–238 (2016). https://doi.org/10.1016/j.apenergy.2016.05.097
7. Jegadheeswaran, S., Pohekar, S.D.: Performance enhancement in latent heat thermal storage system: A review. Renewable and Sustainable Energy Reviews. 13, 2225–2244 (2009). https://doi.org/10.1016/j.rser.2009.06.024
8. Liu, S., Li, Y., Zhang, Y.: Review on Heat Transfer Mechanisms and Characteristics in Encapsulated PCMs. HEAT TRANSFER ENGINEERING. 36, 880–901 (2015). https://doi.org/10.1080/01457632.2015.965093
9. Teggar, M., Ajarostaghi, S.S.M., Yıldız, Ç., Arıcı, M., Ismail, K.A.R., Hakeem Niyas, Niyas, H., Lino, F.A.M., Fatima A.M. Lino, Mert, M.S., Khalid, M.: Performance enhancement of latent heat storage systems by using extended surfaces and porous materials: A state-of-the-art review. Journal of energy storage. (2021). https://doi.org/10.1016/j.est.2021.103340
10. Feng, D., Feng, Y., Qiu, L., Li, P., Zang, Y., Zou, H., Yu, Z., Zhang, X.: Review on nanoporous composite phase change materials: Fabrication, characterization, enhancement and molecular simulation. Renewable and Sustainable Energy Reviews. 109, 578–605 (2019). https://doi.org/10.1016/j.rser.2019.04.041
11. Zhang, S., Feng, D., Shi, L., Wang, L., Jin, Y., Tian, L., Li, Z., Wang, G., Zhao, L., Yan, Y.: A review of phase change heat transfer in shape-stabilized phase change materials (ss-PCMs) based on porous supports for thermal energy storage. Renewable and Sustainable Energy Reviews. 135, 110127 (2021). https://doi.org/10.1016/j.rser.2020.110127
12. Samarskii, A.A., Vabishchevich, P.N., Iliev, O.P., Churbanov, A.G.: Numerical simulation of convection/diffusion phase change problems—a review. International Journal of Heat and Mass Transfer. 36, 4095–4106 (1993). https://doi.org/10.1016/0017-9310(93)90071-D
13. Brent, A.D., Voller, V.R., Reid, K.J.: Enthalpy-Porosity Technique for Modeling Convection-Diffusion Phase Change: Application to the Melting of a Pure Metal. Numerical Heat Transfer. 13, 297–318 (1988). https://doi.org/10.1080/10407788808913615
14. Poirier, D., Salcudean, M.: On Numerical Methods Used in Mathematical Modeling of Phase Change in Liquid Metals. Journal of Heat Transfer. 110, 562–570 (1988). https://doi.org/10.1115/1.3250529
15. Tay, N.H.S., Belusko, M., Bruno, F.: An effectiveness-NTU technique for characterising tube-in-tank phase change thermal energy storage systems. Applied Energy. 91, 309–319 (2012). https://doi.org/10.1016/j.apenergy.2011.09.039
16. Bruno, F., Belusko, M., Tay, N.H.S.: Design of PCM Thermal Storage Systems Using the Effectiveness-NTU Method. In: Proceedings of the EuroSun 2010 Conference. pp. 1–8. International Solar Energy Society, Graz, Austria (2010)
17. Liang, H., Niu, J., Gan, Y.: Performance optimization for shell-and-tube PCM thermal energy storage. Journal of Energy Storage. 30, 101421 (2020). https://doi.org/10.1016/j.est.2020.101421
18. Tian, Y., Zhao, C.: A numerical investigation of heat transfer in phase change materials (PCMs) embedded in porous metals. ENERGY. 36, 5539–5546 (2011). https://doi.org/10.1016/j.energy.2011.07.019

19. Belusko, M., Halawa, E., Bruno, F.: Characterising PCM thermal storage systems using the effectiveness-NTU approach. International Journal of Heat and Mass Transfer. 55, 3359–3365 (2012). https://doi.org/10.1016/j.ijheatmasstransfer.2012.03.018
20. Tay, N.H.S., Belusko, M., Castell, A., Cabeza, L.F., Bruno, F.: An effectiveness-NTU technique for characterising a finned tubes PCM system using a CFD model. Applied Energy. 131, 377–385 (2014). https://doi.org/10.1016/j.apenergy.2014.06.041
21. Stathopoulos, N., El Mankibi, M., Santamouris, M.: Numerical calibration and experimental validation of a PCM-Air heat exchanger model. Applied Thermal Engineering. 114, 1064–1072 (2017). https://doi.org/10.1016/j.applthermaleng.2016.12.045
22. Stathopoulos, N., El Mankibi, M., Issoglio, R., Michel, P., Haghighat, F.: Air–PCM heat exchanger for peak load management: Experimental and simulation. Solar Energy. 132, 453–466 (2016). https://doi.org/10.1016/j.solener.2016.03.030
23. Barz, T., Emhofer, J.: Paraffins as phase change material in a compact plate-fin heat exchanger - Part I: Experimental analysis and modeling of complete phase transitions. Journal of Energy Storage. 33, 102128 (2021). https://doi.org/10.1016/j.est.2020.102128
24. Shon, J., Kim, H., Lee, K.: Improved heat storage rate for an automobile coolant waste heat recovery system using phase-change material in a fin–tube heat exchanger. Applied Energy. 113, 680–689 (2014). https://doi.org/10.1016/j.apenergy.2013.07.049
25. Promoppatum, P., Yao, S.-C., Hultz, T., Agee, D.: Experimental and numerical investigation of the cross-flow PCM heat exchanger for the energy saving of building HVAC. Energy and Buildings. 138, 468–478 (2017). https://doi.org/10.1016/j.enbuild.2016.12.043
26. Frank, J.Y., Borman, D.J., Greiciunas, E., Khan, A., Summers, J.: Phase Change Materials for Absorbing Peak Heat Loads in Aircraft: An Effectiveness-NTU Model for Predicting the Performance of Compact Heat Exchanger. Presented at the ASME 2023 Heat Transfer Summer Conference collocated with the ASME 2023 17th International Conference on Energy Sustainability September 26 (2023)
27. Kays, W.M., London, A.L.: Compact Heat Exchangers. McGraw-Hill Book Company (1964)
28. Vasil, G.M., Proctor, M.R.E.: Dynamic bifurcations and pattern formation in melting-boundary convection. Journal of Fluid Mechanics. 686, 77–108 (2011). https://doi.org/10.1017/jfm.2011.284
29. Favier, B., Purseed, J., Duchemin, L.: Rayleigh–Bénard convection with a melting boundary. Journal of Fluid Mechanics. 858, 437–473 (2019). https://doi.org/10.1017/jfm.2018.773